Computer Physics Communications 320 (2026) 109957

Contents lists available at ScienceDirect

Computer Physics Communications

journal homepage: www.elsevier.com/locate/cpc

Computer Programs in Physics

FukuiGrid: A Python code for c-DFT in solid-state chemistry

Nicolás F. Barrera [a,b,*], Javiera Cabezas-Escares [a,b,*], Mònica Calatayud [c], Francisco Munoz [a,b], Tatiana Gómez [d], Carlos Cárdenas [a,b,*]

[a] Departamento de Física, Facultad de Ciencias, Universidad de Chile, Santiago, Chile
[b] Center for Nanoscience and Nanotechnology (CEDENNA), Manuel Rodríguez Sur 415, Santiago, Chile
[c] Sorbonne Université, MONARIS, CNRS-UMR, 8233, 4 Place Jussieu, F-75005, Paris, France
[d] Theoretical and Computational Chemistry Center, Institute of Applied Chemical Sciences, Faculty of Engineering, Universidad Autónoma de Chile, Santiago, Chile

ARTICLE INFO

The review of this paper was arranged by Dr W Jong

Keywords:
DFT
c-DFT
Reactivity
Solid-state

ABSTRACT

FukuiGrid is a Python-based code that calculates Fukui functions and Fukui potentials in systems with periodic boundary conditions, making it a valuable tool for solid-state chemistry. It focuses on chemical reactivity descriptors from Conceptual Density-Functional Theory (c-DFT) and enables the calculation of Fukui functions through methods such as finite differences and interpolation. FukuiGrid addresses the challenges associated with periodic boundary conditions when calculating the electrostatic potential of a Fukui function (known as the Fukui potential) by integrating various corrections to alleviate the compensating background of charge. These corrections include the electrode approach and self-consistent potential correction as post-processing techniques. This package is compatible with VASP outputs and specifically designed to study the reactivity of surfaces and adsorbates. It generates surface reactivity maps and provides insights into adsorption site preferences, as well as regions prone to electron donation or withdrawal. FukuiGrid has been designed to make c-DFT easier for the surface chemistry community.

1. Introduction

Conceptual Density-Functional Theory (c-DFT) [1–7] is one of the most widely used and highly successful theories of chemical reactivity. Developed under the framework of the physical and mathematical formalism of Density-Functional Theory (DFT), it has been able to provide theoretical support to key principles of chemical reactivity, such as Hard and Soft Acids and Bases (HSAB) principle [8–16] or the maximum hardness principle [17–22], and establishes others such as the "$|\Delta\mu|$ big is good" rule [23,24].

One of the most remarkable features of c-DFT is the emergence of reactivity descriptors from it, e.g., chemical hardness and Fukui functions [25]. The last ones, in particular, are crucial because they quantify the local propensity of a chemical species to exchange electrons, thus providing a spatially-resolved view of an inherent chemical reactivity [4,26].

The success of c-DFT has been demonstrated in studying chemical systems with open-boundary conditions, such as atoms, molecules, clusters, etc. However, its use in solid-state reactivity has been limited due to theoretical and computational challenges arising from degeneracies and periodic boundary conditions (PBC) found in extended systems and solids [27–29,29–39]. One of these significant challenges is the inclusion of a homogeneous compensating background charge (CBC) to compute electrostatic contributions in charged supercells [40,41]. The CBC has consequences for both the self-consistent density and the electrostatic potential, leading to artificial alterations in chemical descriptors. These changes complicate using c-DFT for both qualitative and quantitative purposes in solid-state systems [29,39].

This paper focuses on the presentation of FukuiGrid, an open-source Python code designed to calculate and analyze response functions and related quantities derived from c-DFT in solid-state systems. FukuiGrid is capable of performing several tasks including the calculation of Fukui functions from finite differences and interpolation method, calculation and correction of Fukui potential using the electrodes' method [42,43] and Self-Consistent Potential Correction (SCPC) [44], the computation of interaction energy between a chemical species, whose reactive site is modelled as a point charge, Anderson et al. [45,46] and a surface using a perturbation expansion of c-DFT, and various grid data processing tasks. In reference [39] the reader will find a comprehensive study in which many of these capacities are used to characterize the chemical reactivity of a diverse range of metallic and semiconductor surfaces, including elemental metals such as Ti and Pt, metal oxides likeTiO_2, SnO_2, and MgO, and transition metal carbides such as TiC and ZrC.

* Corresponding authors.
E-mail addresses: nicolas.barrera@ug.uchile.cl (N.F. Barrera), javiera.cabezas.e@ug.uchile.cl (J. Cabezas-Escares), cardena@uchile.cl (C. Cárdenas).

https://doi.org/10.1016/j.cpc.2025.109957
Received 2 September 2025; Received in revised form 7 November 2025; Accepted 13 November 2025
Available online 27 November 2025

Several software packages, including PRIMoRDiA [47], UCA-Fukui [48], PyGlobal [49], Multiwfn [50,51], ADF (Conceptual DFT module) [52], and ChemTools [53], have been designed for the analysis of conceptual-DFT properties in systems with open boundary condition. These tools have significantly advanced the study of molecular reactivity and electronic structure in finite systems. FukuiGrid, in contrast, extends these capabilities to periodic boundary conditions, making it possible to study chemical reactivity within condensed-phases and extended materials.

The remainder of this article is organized as follows. In Section 2, we briefly describe the FukuiGrid architecture. Some illustrated examples and their connection to the theory are presented in Section 3. We conclude in Section 4.

2. Code overview

2.1. Some features

FukuiGrid is designed as an interactive tool that provides step-by-step messages to guide users through the available actions and required inputs (pipeline). Therefore, memorizing complex keywords or command line syntax is unnecessary, making it more accessible for both beginners and experienced users. Special attention has been given to ensuring an intuitive user experience while maintaining flexibility and advanced functionality.

By default, FukuiGrid generates graphical representations for various tasks; however, its primary outputs are charge densities and electrostatic potentials, saved in `CHGCAR` and `LOCPOT` formats, respectively. These formats are widely compatible with solid-state visualization software such as VESTA [54], XCrysDen [55,56], and VMD [57]. Additionally, these files can be used for other analyses, such as topological studies performed with tools like Bader [58–61], Critic2 [62,63], or TopChem2 [64] programs.

2.2. FukuiGrid architecture

The architecture of FukuiGrid is organized into three main sections:

- Utility Functions: These functions handle specific tasks that support the code's primary operations and overall workflow. Tasks include reading and processing input files, applying filters, transforming data, and writing output files.
- Main Functions: These are the core functionalities offered to the user. Each function is documented with a header that details the required inputs, generated outputs, a brief description, and relevant process information. These functions represent the principal tasks displayed to the user when the code is executed.
- Main Menu: This section is the entry point when the code is executed. It provides an interactive menu where users can select and execute processes from a list of available options.

Both the utility and main functions are designed to be reusable and can be invoked externally by importing the FukuiGrid module. Additionally, the main functions can be executed directly with single-line commands.

The data flow within FukuiGrid is illustrated in Fig. 1. Input files, such as `LOCPOT` and `CHGCAR` generated by the VASP package [65–68], are processed by the main functions to produce various outputs, including new text files in VASP or plain-text formats. VASP-formatted output files can be used as inputs for subsequent main function executions and visualized using tools like VESTA [54]. Furthermore, some functions export planar averages, heatmaps, and other visualizations (e.g., .png and .txt formats) to enhance understanding of the methods.

2.3. Source code

The project's GitHub repository is located at https://github.com/cacarden/FukuiGrid. Documentation with examples can be found there. FukuiGrid is supported by Python 3.X.

3. FukuiGrid functions and examples

This section presents an overview of the main options of FukuiGrid, describing their theoretical background and practical applications. Illustrative examples are provided to showcase their practical application and demonstrate how FukuiGrid can be used to analyze and compute reactivity descriptors in periodic systems. Additionally, the FukuiGrid GitHub repository contains a dedicated section with detailed Hands-On tutorials for each function, along with the corresponding input and output files.

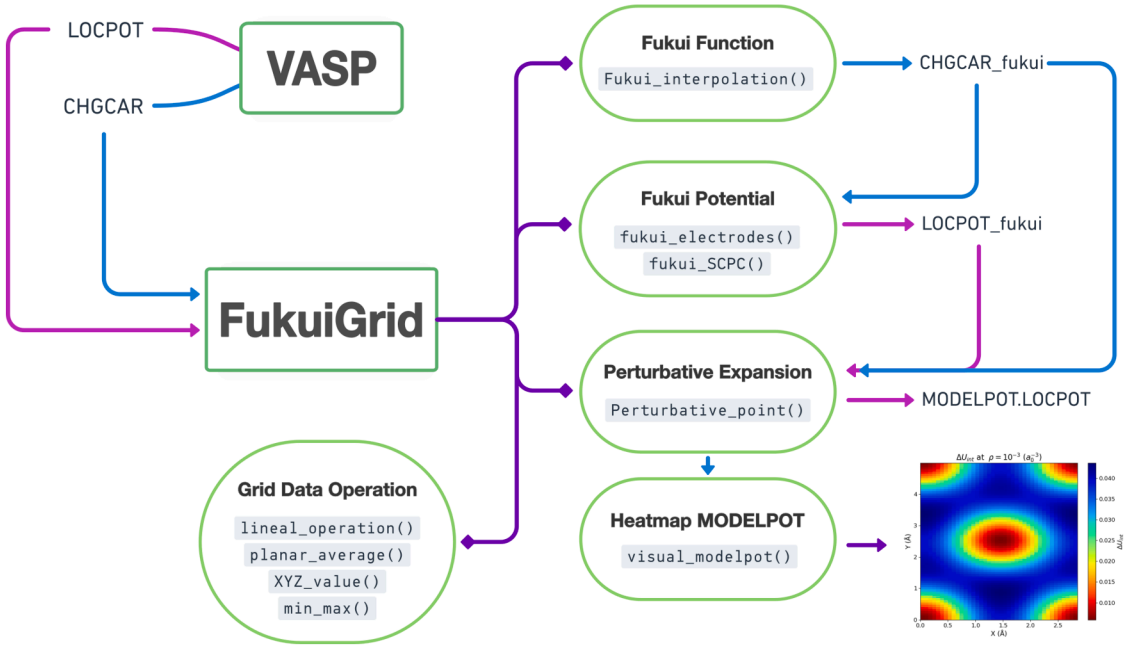

Fig. 1. FukuiGrid code structure.

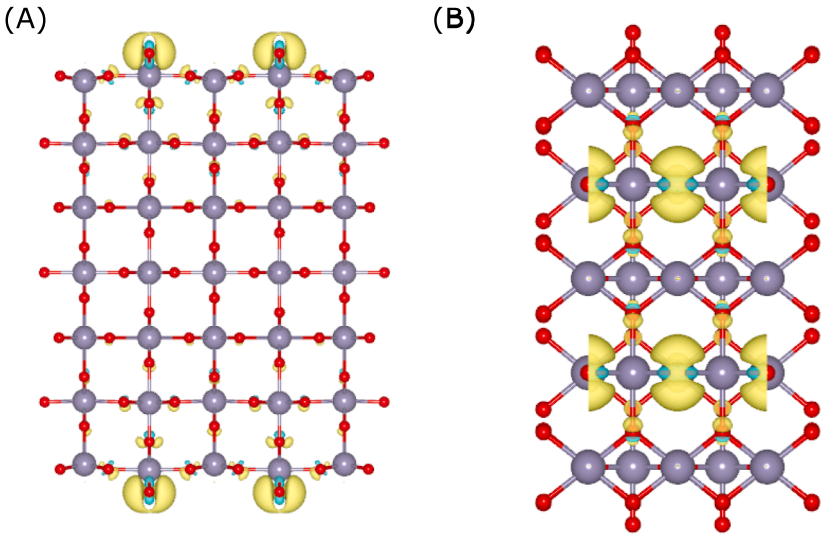

Fig. 2. Isosurface maps (± 0.002 a_0^{-3}) of electrophilic Fukui functions $f^-(\mathbf{r})$ of rutile SnO_2 (110) surface. Panels A and B show side and top views, respectively, for a 2x2 slab model.

3.1. *Fukui functions,* $f^{\pm}(\vec{r})$

`Option 1 - Fukui Function` of FukuiGrid allows calculating Fukui functions by the interpolation method [29]. Fukui functions, $f^{\pm}(\vec{r})$, are the response of electron density to the change in the number of electrons when the external potential is kept fixed, Parr and Yang [25], Ayers and Levy [26], Yang et al. [69], Fievez et al. [70], Fuentealba et al. [71]

$$f^{\pm}(\vec{r}) = \left(\frac{\partial\rho(\vec{r})}{\partial N}\right)^{\pm}_{v} \tag{1}$$

Due to the discontinuity of $E(N)$, [72] two functions were introduced depending on whether they are calculated just below or above an integer value, giving rise to an electrophilic Fukui function, $f^-(\vec{r})$, and a nucleophilic Fukui function, $f^+(\vec{r})$. These functions locally quantify the propensity of a chemical system to exchange electrons. As a further consequence of the aforementioned discontinuity, the Fukui functions are the difference between the density of the actual system and its vertical ions,

$$f^{\pm}(\vec{r}) = \pm\left(\rho_{N\pm1}(\vec{r}) - \rho_N(\vec{r})\right) \tag{2}$$

This definition brings a challenge for periodic systems, since it involves calculating the electronic structure of a supercell with a net charge, which has a divergent electrostatic interaction energy. Solid-state codes that use PBCs and plane-wave basis sets typically address this issue by incorporating a homogeneous compensating background charge (CBC) to maintain charge neutrality [40,41]. However, this means considering a non-physical contribution to the potential into the SCF calculation. To overcome this difficulty, Cerón et al. [29] proposed an interpolation method in which calculations with fractional charges are required, rather than using systems with charges of ±1 electron. The slope of this interpolation at each point corresponds to the Fukui function,

$$\rho(\vec{r}, N) = \rho(\vec{r}r, N_0) + \left(\frac{\partial\rho(\vec{r}, N)}{\partial N}\right)_{v(\vec{r})}\left(N - N_0\right) + \cdots \tag{3}$$

The option 1 in our code performs the linear interpolation using four points for each grid point in real space. Specifically, four `CHGCAR` files with δN = values of 0.00, ±0.05, ±0.10, ±0.15 $|e|$ are required by default, where the sign of the step depends on the type of Fukui function being calculated. The default values of δN were chosen to ensure both the linearity of the $\rho(\mathbf{r})$-N relationship and the numerical stability of the finite-difference scheme [29]. These values can be easily modified by the user if needed. The resulting Fukui function is saved in a file named "`CHGCAR_FUKUI.vasp`" in `CHGCAR` format. Detailed information about the grids used for the calculation is also displayed on the screen.

It is worth mentioning that the implementation of this function in FukuiGrid is significantly more computationally efficient than one previously published by some of us Cerón et al. [29].

Fig. 2 shows the isosurface maps of the Fukui function $f^-(\vec{r})$ of rutile SnO_2 (110) surface, calculated using option 1. The plot indicates that surface bridging oxygens are the sites prone to lose electrons upon electrophilic attack, or in other words, by an oxidizing agent. This is an expected result, as bridging oxygens are surface atoms rich in loosely bound electrons, making them highly susceptible to oxidation.

3.2. *Fukui potential via electrodes*

The Fukui potential [73–75,75,76] corresponds to an electrostatic potential due to a charge density equal to a Fukui function. It can shed light on whether those regions in which the system is more prone to accept or donate electrons from/to the reactant are accessible to it Fuentealba and Cárdenas [3], Cárdenas et al. [75], Gómez et al. [77], Osorio et al. [78], Munoz and Cardenas [79], Muñoz et al. [80]. It is given by,

$$v_f^{\pm}(\vec{r}) = \int \frac{f^{\pm}(\vec{r'})}{|\vec{r'} - \vec{r}|}\, d\vec{r'}. \tag{4}$$

Like the Fukui functions, the Fukui potential can be computed as a finite difference of electrostatic potentials of electron densities, i.e.,

$$v_f^{\pm}(\vec{r}) = \pm\left(\Phi_N(\vec{r}) - \Phi_{N\pm1}(\vec{r})\right) \tag{5}$$

Here,

$$\Phi_N(\vec{r}) = \sum_{\alpha}\frac{Z_\alpha}{|\vec{R}_\alpha - \vec{r}|} - \int\frac{\rho_N(\vec{r'})}{|\vec{r'} - \vec{r}|}\, d\vec{r'} \tag{6}$$

denotes the electrostatic potential of the system with N electrons. Although the calculation via Eq. (5) is straightforward, errors are introduced when this equation is used with calculations with PBC and a discrete plane-wave basis set in which the charged systems involve the CBC. These errors arise because, to exploit the periodic nature of the potential, the Hartree contribution is calculated using a Fourier series,

$$V(\vec{r}) = \frac{4\pi}{\Omega}\sum_{\vec{G}\neq0}\frac{n(\vec{G})}{G^2}e^{i\vec{G}\cdot\vec{r}}. \tag{7}$$

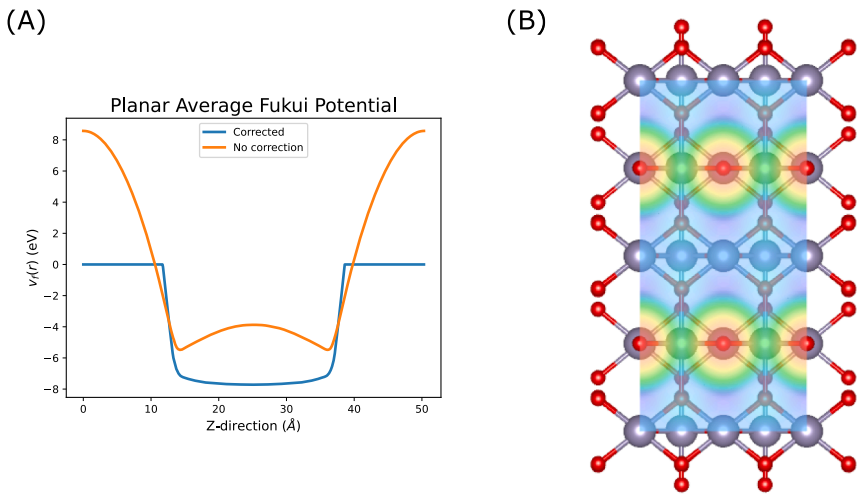

Fig. 3. Panel A shows the planar averages of the uncorrected Fukui potential (orange) and the corrected Fukui potential via electrodes' method (light blue) along the aperiodic direction of the slab model for the rutile SnO_2 (110) surface. Panel B displays a Fukui potential map, illustrating a top view of an electronic density isosurface of $10^{-3}\ a_0^{-3}$, colored according to the Fukui potential $v_f^-(\vec{r})$, for a 2×2 slab model.

where the null wave vector ($\vec{G}=0$) is excluded from the sum to avoid divergence of the potential. In the case of a neutral cell, this exclusion is unproblematic, as $V(\vec{G}=0)$ corresponds to the average potential, which can be set to zero due to charge neutrality, where the total electronic and ionic charges cancel each other. For charged cells, the neutrality is restored by adding a homogeneous CBC ($-\langle n(\mathbf{r})\rangle$),

$$n(\vec{r}) \longrightarrow n(\vec{r}) - \langle n(\vec{r})\rangle. \tag{8}$$

generating a fictitious or non-physical contribution to the potential that needs to be corrected [44,81–84].

`Option 2 - Fukui Potential via Electrodes` computes and corrects the Fukui potential via the electrodes' method, which separates the electrostatic potential into the real slab potential and the contribution from the CBC, assuming the validity of the superposition principle [39,42,43]. The CBC potential, screened by the dielectric profile of the slab, is determined using the Poisson equation,

$$\frac{d}{dz}\left(\varepsilon(z)\frac{d}{dz}V_{CBC}(z)\right) = -n_{CBC}, \tag{9}$$

with boundary conditions imposed by grounded reference electrodes at the supercell edges. Both the dielectric profile limits of the slab model and the zero are determined according to what we have previously reported [39].

This Function requires both the charge density file of the Fukui function (from which its generated electrostatic potential is calculated) and the charge density of the neutral slab model. The latter is used to determine both the amplitude and spatial position of the dielectric profile and the zero of the generated Fukui potential; a more detailed discussion about this can be found in our recent article [39]. Moreover, it is important to mention that the macroscopic dielectric constant of the material can be calculated using density functional perturbation theory by specifying `LEPSILON=.TRUE.` in `INCAR` file; more details about this can be found in the FukuiGrid GitHub repository.

Fig. 3 panel A shows the planar averages of the uncorrected (orange) and electrode-corrected (light blue) Fukui potentials, $v_f^-(\vec{r})$ of rutile SnO_2 (110) surface. In this case, the Fukui function $f^-(\vec{r})$ is obtained by interpolation. This graph is automatically generated when option 2 is executed, together with the file "`FUKUI_LOCPOT.vasp`" containing the corrected Fukui potential in `LOCPOT` format. On the other hand, panel B of Fig. 3 shows a map of the Fukui potential on the $10^{-3}\ a_0^{-3}$ electron density isosurface, generated using VESTA. It can be seen that, for this isosurface, the potential values are, in magnitude, larger in the vicinity of the two-fold coordinated bridging oxygens.

3.3. Fukui potential via SCPC

`Option 3 - Fukui Potential via SCPC` also calculates and corrects the Fukui potential. However, in this case, the correction is computed with the Self-Consistent Potential Correction (SCPC) method [44,85], which eliminates interactions with the CBC by applying a self-consistently updated correction to the electrostatic potential during the solution of the Kohn-Sham equations. This scheme is provided by its developers as a patch for VASP [44,85]. Among the files provided, the `z-vcor.dat` file contains the planar average of potential along the Z direction (non-periodic direction of the slab model) using a coarse grid. FukuiGrid reads this file, interpolates the correction onto the finer grid of the Fukui potential, and uses it to correct the Fukui potential obtained through Eq. (7).

Fig. 4 panel A shows the planar averages of the uncorrected (orange) and corrected via SCPC method (light blue) Fukui potentials, $v_f^-(\vec{r})$, for the Fukui function $f^-(\vec{r})$ of the rutile SnO_2 (110) surface. This graph is generated by option 3 along with the file "`FUKUI_LOCPOT.vasp`" in `LOCPOT` format. Panel B shows the Fukui potential map on the $10^{-3}\ a_0^{-3}$ electron density isosurface, generated with VESTA, highlighting larger potential values near the bridging oxygens.

3.4. Grid data operations

`Option 4 - Grid Data Operations` is designed to manipulate `CHGCAR` and `LOCPOT` files. It performs several operations, including:

- Adding or subtracting two files.
- Scaling data by a factor.
- Adding a constant to the data.
- Calculating planar averages.
- Converting data to `X,Y,Z,value` format.
- Finding maximum and minimum values.

These operations can be used to determine the Fukui functions (see Eq. (2)) and the work function, to name a few examples. Some of these functions can be found in post-processing software such as Multwfn [50,51] or VASPKIT [86], and through the Henkelman group's scripts [87].

As an example, Fig. 5 shows the planar average of the valence electron density along the X-direction of the rutile SnO_2 (110) surface model. FukuiGrid generates this graph along with a file named `PA_ED.dat` containing the position and planar average for all grid points in that particular direction.

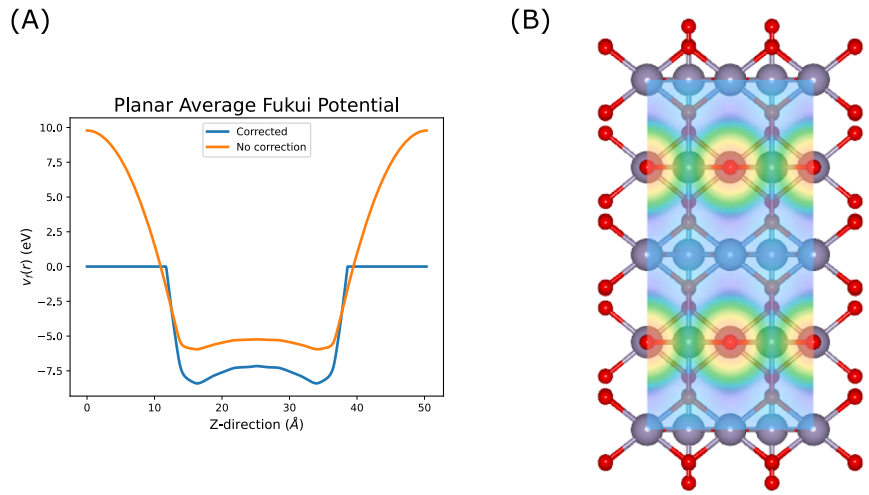

Fig. 4. Panel A shows the planar averages of the uncorrected Fukui potential (orange) and the corrected Fukui potential via SCPC method (light blue) along the aperiodic direction of the slab model for the rutile SnO_2 (110) surface. Panel B displays a Fukui potential map, illustrating a top view of an electronic density isosurface of $10^{-3}\ a_0^{-3}$, colored according to the Fukui potential $v_f^-(\vec{r})$, for a 2x2 slab model.

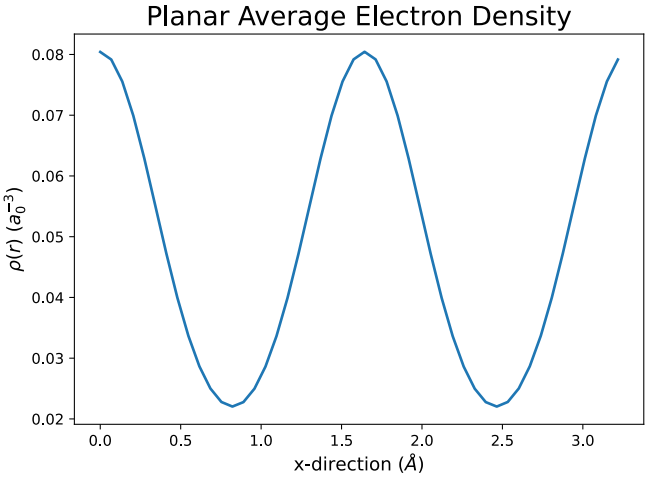

Fig. 5. Planar average of the valence electron density along the x-direction of the rutile SnO_2 (110) surface model, as calculated by FukuiGrid.

3.5. Perturbative expansion

The theoretical framework of c-DFT allows chemical interactions and reactions to be viewed as processes in which the number of electrons, N, and the reacting species' external potential, v, are modified. From this perspective, it is possible to obtain a perturbative expansion of the energy, which is given by Ayers and Levy [26]:

$$\begin{aligned}\Delta U = &\left(\frac{\partial E}{\partial N}\right)_v \Delta N + \int \left[\frac{\partial E}{\partial v(\vec{r})}\right]_N \delta v(\vec{r}) d\vec{r} + \cdots \\ &+ \int \left(\frac{\partial}{\partial N}\right)_v \left[\frac{\delta E}{\delta v(\vec{r})}\right]_N \Delta N \delta v(\vec{r}) d\vec{r} + \cdots \\ &+ \int \left[\frac{\partial V_{NN}}{\partial v(\vec{r})}\right]_N \delta v(\vec{r}) d\vec{r}.\end{aligned} \tag{10}$$

FukuiGrid allows one to make use of this expansion by modelling the change in external potential as a point charge, q, Anderson et al. [45] and considering only the terms that depend locally and changes up to first order in the external potential, giving the following simple expression at 0 K:

$$\begin{aligned}\Delta U(\vec{r}) &= q \underbrace{\sum_\alpha \frac{Z_\alpha}{|\vec{R}_\alpha - \vec{r}|} - \int \frac{q\rho(\vec{r'})}{|\vec{r} - \vec{r'}|} d\vec{r'}}_{\Phi(\vec{r})} - \Delta N q \underbrace{\int \frac{f^{\pm}(\vec{r'})}{|\vec{r} - \vec{r'}|} d\vec{r'}}_{v_f^{\pm}(\vec{r})} \\ &= q\Phi(\vec{r}) - q\Delta N v_f^{\pm}(\vec{r}),\end{aligned} \tag{11}$$

where $\Phi(\vec{r})$ and $v_f^{\pm}(\vec{r})$ are the (molecular) electrostatic potential and the Fukui potential, respectively. In this model, the reactivity of a system is probed using a point charge, which acts as a probe for the chemical reactivity of the system. If there is no change in ΔN, the electrostatics controls reactivity. In contrast, if ΔN changes, the Fukui potential, $v_f^{\pm}(\vec{r})$, accounts for the local variation in reactivity due to an electron-transfer process.

This function requires both the electrostatic potential of the surface and the Fukui potential, along with the parameters q and ΔN, which measure the charge and electron transfer of the probe, respectively. Additionally, for the optional generation of the reactivity map on a surface of constant density, the charge density of the surface must be provided.

Heatmaps illustrating the spatial distribution of the interaction energy between a probe, modelled as a point charge, and the rutile SnO_2 (110) surface are shown in Fig. 6. The panels depict how the interaction energy varies depending on the values of q and ΔN, representing different charge transfer scenarios. As expected, changes in these parameters significantly alter the energy landscape, modifying the most and least favourable regions for interaction. These maps provide a clear visualization of how electrostatic and Fukui potential contributions influence surface reactivity, offering insights into adsorption site preferences.

It is worth mentioning that, as some of us have previously discussed [39], this simple perturbative model can be useful for predicting the reactivity of surfaces to oxidizing and reducing agents. In particular, we have shown that it can accurately predict the adsorption sites of Na and Cl atoms on a rutile TiO_2 (110) surface, with a good correlation with the interaction energies calculated at the theoretical level of the PBE functional.

3.6. Computational details

To evaluate the functions of FukuiGrid, all PBC DFT calculations were performed with the Vienna Ab initio simulation package (VASP) [65–68] Version 6.2.1. The Projector Augmented Wave (PAW) method was used to describe the core electrons with 16 and 6 valence electrons

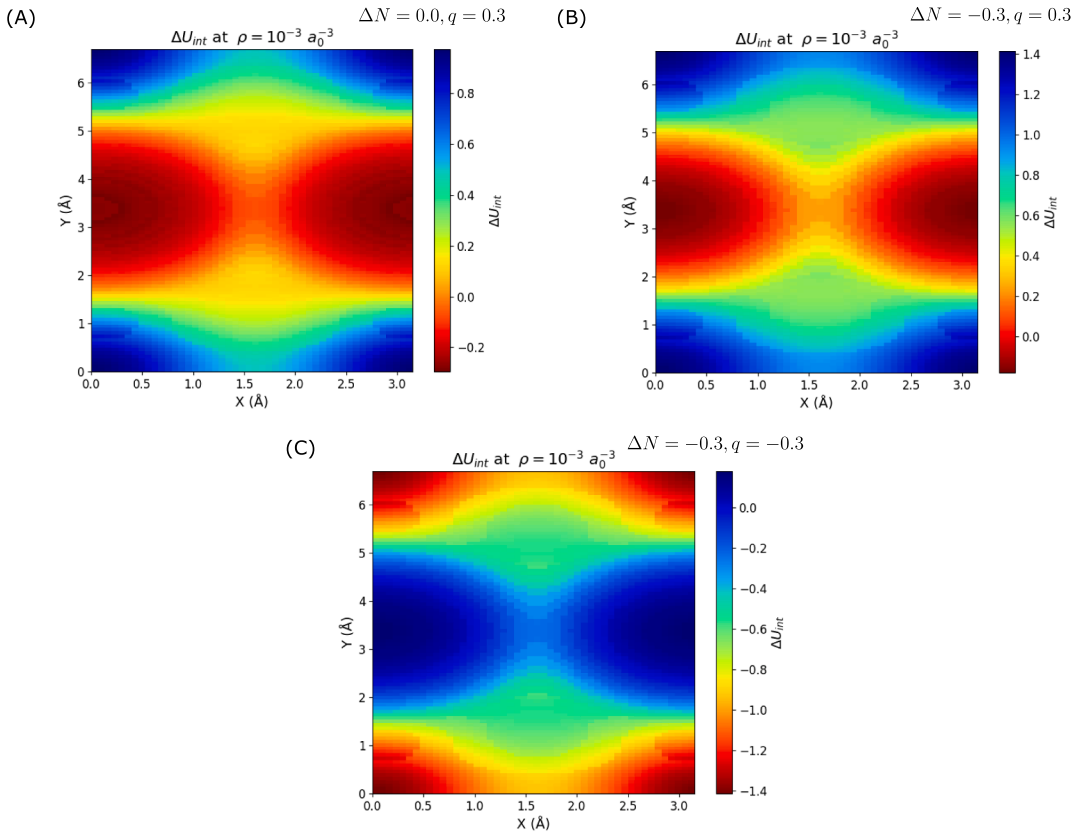

Fig. 6. Heatmaps of the interaction energy between a probe (modelled as a point charge) and the rutile SnO_2 (110) surface, shown in three panels (A, B, and C). Each panel represents different values of electron-transfer (ΔN) and point charge (q) parameters, in $|e|$, over the $10^{-3}a_0^{-3}$ isosurface. In panel (A), $\Delta N = 0.0, q = 0.3$; in panel (B), $\Delta N = -0.3, q = 0.3$; and in panel (C), $\Delta N = -0.3, q = -0.3$. The heatmaps illustrate the spatial distribution of the interaction energy between the point charge and the surface using Eq. (11).

for Sn and O, respectively [88,89]. The GGA Perdew-Burke-Ernzerhof (PBE) exchange-correlation functional was used [90], and the plane-wave basis set was truncated at 700 eV for all systems. For sampling the reciprocal space, the Monkhorst-Pack scheme [91] was chosen, using $6 \times 6 \times 1$ **k**-point mesh for SnO_2 (110). The GGA + U approach of Dudarev et al. [92] was used to treat the 4d electrons of Sn. We chose the effective Hubbard on-site Coulomb interaction parameter ($U' = U - J$) to be 3.5 eV, according to the proposed value from previous work [93]. VESTA software [54] was used for all visualizations shown in this article.

4. Conclusion

FukuiGrid is a user-friendly, open-source Python code specifically designed for the calculation of Fukui functions, Fukui potentials, and interaction energy models derived from Conceptual Density Functional Theory (c-DFT) in periodic systems. By addressing key challenges such as background charge corrections and electrostatic potential alignments.

The code is fully compatible with VASP outputs and provides a straightforward workflow for visualization and analysis. One of its key features is the ability to generate reactivity maps, which help identifying the most and least favourable adsorption sites based on the electrostatic and Fukui potentials. This makes FukuiGrid especially useful for studying catalytic processes, adsorption phenomena, and chemical reactivity trends in solid-state chemistry.

FukuiGrid is available at https://github.com/cacarden/FukuiGrid, along with detailed documentation, Hands-On tutorials, and example datasets. We hope this tool will serve as a valuable resource for advancing solid-state chemistry and surface science research.

Declaration of generative AI in scientific writing

During the preparation of this work, N.B. used ChatGPT and Perplexity to improve the clarity of the writing. After using this tool/service, the authors reviewed and heavily edited the content as needed and take full responsibility for the content of the published article.

CRediT authorship contribution statement

Nicolás F. Barrera: Writing – review & editing, Writing – original draft, Supervision, Software, Methodology, Investigation, Formal analysis, Conceptualization; **Javiera Cabezas-Escares:** Writing – review & editing, Writing – original draft, Software, Methodology, Investigation, Formal analysis; **Mònica Calatayud:** Writing – review & editing, Supervision, Methodology, Investigation, Conceptualization; **Francisco Munoz:** Writing – review & editing, Validation, Investigation, Funding acquisition; **Tatiana Gómez:** Writing – review & editing, Methodology, Investigation, Funding acquisition, Conceptualization; **Carlos Cárdenas:** Writing – review & editing, Writing – original draft, Validation, Supervision,Software, Resources, Project administration, Methodology, Investigation, Funding acquisition, Formal analysis, Conceptualization.

Data availability

Data will be made available on request.

Declaration of competing interest

The authors declare that they have no known competing financial interests or personal relationships that could have appeared to influence the work reported in this paper.

Acknowledgements

This research was funded by FONDECYT through projects 1220366, 1260430, 1260992, 1231487, and by the Center for Nanoscience and Nanotechnology, CEDENNA CIA 250002. NFB gratefully acknowledges ANID for their national master's scholarship year 2022 number 22220676. CC acknowledges ANID for the grant ECOS210019. JCE gratefully acknowledges ANID for her national doctoral scholarship year 2023 number 21231429. Powered@NLHPC: This research/thesis was partially supported by the supercomputing infrastructure of the NLHPC (CCSS210001). This work was performed using HPC resources from GENCI-IDRIS (grants 2023-A0150802131, 2024-A0170802131).

References

[1] H. Chermette, Chemical reactivity indexes in density functional theory, J. Comput. Chem. 20 (1) (1999) 129–154.
[2] P. Geerlings, F. De Proft, W. Langenaeker, Conceptual density functional theory, Chem. Rev. 103 (5) (2003) 1793–1873.
[3] P. Fuentealba, C. Cárdenas, Density functional theory of chemical reactivity, in: Chemical Modelling: Volume 11, The Royal Society of Chemistry, 2014, pp. 151–171.
[4] S.-B. Liu, Conceptual density functional theory and some recent developments, Acta Phys. Chim. Sin. 25 (3) (2009) 590–600.
[5] P. Geerlings, F. De Proft, Conceptual DFT: the chemical relevance of higher response functions, Phys. Chem. Chem. Phys. 10 (21) (2008) 3028–3042.
[6] J. Gazquez, Perspectives on density functional theory of chemical reactivity, J. Mex. Chem. Soc. 52 (1) (2008) 3–10.
[7] P. Geerlings, E. Chamorro, P.K. Chattaraj, F. De Proft, J.L. Gázquez, S.B. Liu, C. Morell, A. Toro-Labbé, A. Vela, P. Ayers, Conceptual density functional theory: status, prospects, issues, Theor. Chem. Acc. 139 (2) (2020).
[8] R.G. Pearson, Hard and soft acids and bases, J. Am. Chem. Soc. 85 (22) (1963) 3533–3539.
[9] R.G. Pearson, Hard and soft acids and bases, HSAB, part 1: fundamental principles, J. Chem. Educ. 45 (9) (1968) 581–586.
[10] R.G. Pearson, Hard and soft acids and bases, HSAB, part II: underlying theories, J. Chem. Educ. 45 (10) (1968) 643–647.
[11] P.K. Chattaraj, H. Lee, R.G. Parr, HSAB principle, J. Am. Chem. Soc. 113 (5) (1991) 1855–1856.
[12] P.W. Ayers, R.G. Parr, R.G. Pearson, Elucidating the hard/soft acid/base principle: a perspective based on half-reactions, J. Chem. Phys. 124 (19) (2006) 194107.
[13] P.W. Ayers, The physical basis of the hard/soft acid/base principle, Faraday Discuss. 135 (2007) 161–190.
[14] C. Cardenas, P.W. Ayers, How reliable is the hard–soft acid–base principle? An assessment from numerical simulations of electron transfer energies, Phys. Chem. Chem. Phys. 15 (2013) 13959–13968.
[15] P.W. Ayers, C. Cardenas, Communication: a case where the hard/soft acid/base principle holds regardless of acid/base strength, J. Chem. Phys. 138 (18) (2013) 181106.
[16] R.A. Miranda-Quintana, T.D. Kim, C. Cárdenas, P.W. Ayers, The HSAB principle from a finite-temperature grand-canonical perspective, Theor. Chem. Acc. 136 (12) (2017) 135.
[17] R.G. Pearson, R. G, Recent advances in the concept of hard and soft acids and bases, J. Chem. Educ. 64 (7) (1987) 561–567.
[18] R.G. Parr, P.K. Chattaraj, Principle of maximum hardness, J. Am. Chem. Soc. 113 (5) (1991) 1854–1855.
[19] R.G. Pearson, W.E. Palke, Support for a principle of maximum hardness, J. Phys. Chem. 96 (8) (1992) 3283–3285.
[20] P.W. Ayers, R.G. Parr, Variational principles for describing chemical reactions: the Fukui function and chemical hardness revisited, J. Am. Chem. Soc. 122 (9) (2000) 2010–2018.
[21] M. Torrent-Sucarrat, J.M. Luis, M. Duran, M. Sola, On the validity of the maximum hardness and minimum polarizability principles for nontotally symmetric vibrations, J. Am. Chem. Soc. 123 (32) (2001) 7951–7952.
[22] R.A. Miranda-Quintana, P.W. Ayers, Note: maximum hardness and minimum electrophilicity principles, J. Chem. Phys. 148 (19) (2018) 196101.
[23] R.G. Parr, Y. Weitao, Density-functional theory of atoms and molecules, International Series of Monographs on Chemistry, Oxford University Press, 1994.
[24] R.A. Miranda-Quintana, F. Heidar-Zadeh, P.W. Ayers, Elementary derivation of the "$|\Delta\mu|$ big is good" rule, J. Phys. Chem. Lett. 9 (15) (2018) 4344–4348.
[25] R.G. Parr, W. Yang, Density functional approach to the frontier-electron theory of chemical reactivity, J. Am. Chem. Soc. 106 (14) (1984) 4049–4050.
[26] P.W. Ayers, M. Levy, Perspective on "density functional approach to the frontier-electron theory of chemical reactivity" Parr RG, Yang W (1984) J Am Chem Soc 106: 4049–4050, Theor. Chem. Acc. 103 (2000) 353–360.
[27] M.H. Cohen, M.V. Ganduglia-Pirovano, J. Kudrnovský, Electronic and nuclear chemical reactivity, J. Chem. Phys. 101 (10) (1994) 8988–8997.
[28] M.H. Cohen, A. Wasserman, On the foundations of chemical reactivity theory, J. Phys. Chem. A 111 (11) (2007) 2229–2242.
[29] M.L. Cerón, T. Gomez, M. Calatayud, C. Cárdenas, Computing the fukui function in solid-state chemistry: application to alkaline earth oxides bulk and surfaces, J. Phys. Chem. A 124 (14) (2020) 2826–2833.
[30] C. Cardenas, F. De Proft, E. Chamorro, P. Fuentealba, P. Geerlings, Theoretical study of the surface reactivity of alkaline earth oxides: local density of states evaluation of the local softness, J. Chem. Phys. 128 (3) (2008) 034708.
[31] C. Cardenas, P.W. Ayers, A. Cedillo, Reactivity indicators for degenerate states in the density-functional theoretic chemical reactivity theory, J. Chem. Phys. 134 (17) (2011) 174103.
[32] P. Bultinck, C. Cardenas, P. Fuentealba, P.A. Johnson, P.W. Ayers, How to compute the Fukui matrix and function for systems with (quasi-)degenerate states, J. Chem. Theory Comput. 10 (1) (2013) 202–210.
[33] P. Bultinck, C. Cardenas, P. Fuentealba, P.A. Johnson, P.W. Ayers, Atomic charges and the electrostatic potential are ill-defined in degenerate ground states, J. Chem. Theory. Comput. 9 (2013) 4779–4788.
[34] P. Bultinck, D. Jayatilaka, C. Cardenas, A problematic issue for atoms in molecules: impact of (quasi-)degenerate states on quantum theory atoms in molecules and hirshfeld-I properties, Comput. Theor. Chem. 1053 (0) (2015) 106–111.
[35] C. Cardenas, M. Muñoz, J. Contreras, P.W. Ayers, T. Gómez, P. Fuentealba, Understanding chemical reactivity in extended systems: exploring models of chemical softness in carbon nanotubes, Acta Phys.-Chimica Sinca 34 (2018) 631–638.
[36] A. Cedillo, C. Cárdenas, Reactivity of carbon molecular clusters from a Hückel-type model, J. Phys. Chem. A 123 (40) (2019) 8696–8701. https://doi.org/10.1021/acs.jpca.9b07934 Cedillo, Andres Cardenas, Carlos eng 2019/09/17 J Phys Chem A. 2019 Oct 10;123(40):8696-8701. Epub 2019 Sep 26.
[37] C. Cárdenas, A. Echeverry, T. Novoa, A. Robles-Navarro, T. Gomez, P. Fuentealba, The Fukui Function in Extended Systems: Theory and Applications, John Wiley I& Sons, Ltd, 2022, pp. 555–571.
[38] A.L. Gunton, S.J. Jenkins, Chemical softness in aromatic adsorption: benzene, nitrobenzene and anisole on Pt 111, J. Phys. Chem. A 128 (30) (2024) 6296–6304.
[39] N.F. Barrera, J. Cabezas-Escares, F. Munoz, W.A. Muriel, T. Gomez, M. Calatayud, C. Cardenas, Fukui function and Fukui potential for solid-state chemistry: application to surface reactivity, J. Chem. Theory Comput. 21 (6) (2025) 3187–3203.
[40] M.C. Payne, M.P. Teter, D.C. Allan, T.A. Arias, J.D. Joannopoulos, Iterative minimization techniques for ab initio total-energy calculations: molecular dynamics and conjugate gradients, Rev. Mod. Phys. 64 (4) (1992) 1045.
[41] G. Makov, M.C. Payne, Periodic boundary conditions in ab initio calculations, Phys. Rev. B 51 (7) (1995) 4014.
[42] A.Y. Lozovoi, A. Alavi, J. Kohanoff, R.M. Lynden-Bell, Ab initio simulation of charged slabs at constant chemical potential, J. Chem. Phys. 115 (4) (2001) 1661–1669.
[43] H.-P. Komsa, A. Pasquarello, Finite-size supercell correction for charged defects at surfaces and interfaces, Phys. Rev. Lett. 110 (2013) 095505.
[44] M.C. Da Silva, M. Lorke, B. Aradi, M.F. Tabriz, T. Frauenheim, A. Rubio, D. Rocca, P. Deák, Self-consistent potential correction for charged periodic systems, Phys. Rev. Lett. 126 (7) (2021) 076401.
[45] J.S.M. Anderson, J. Melin, P.W. Ayers, Conceptual density-functional theory for general chemical reactions, including those that are neither charge nor frontier-orbital controlled. I. theory and derivation of a general-purpose reactivity indicator, J. Chem. Theory Comput. 3 (2007) 358–374.
[46] J.S.M. Anderson, J. Melin, P.W. Ayers, Conceptual density-functional theory for general chemical reactions, including those that are neither charge- nor frontier-orbital-controlled. 2. Application to molecules where frontier molecular orbital theory fails, J. Chem. Theory Comput. 3 (2007) 375–389.
[47] I.B. Grillo, G.A. Urquiza-Carvalho, G.B. Rocha, PRIMoRDiA: a software to explore reactivity and electronic structure in large biomolecules, J. Chem. Inf. Model. 60 (12) (2020) 5885–5890.
[48] J. Sánchez-Márquez, D. Zorrilla, A. Sánchez-Coronilla, D.M. de los Santos, J. Navas, C. Fernández-Lorenzo, R. Alcántara, J. Martín-Calleja, Introducing "UCA-FUKUI" software: reactivity-index calculations, J. Mol. Model. 20 (11) (2014) 2492.
[49] S.R. Nath, S.S. Kurup, K.A. Joshi, PyGlobal: a toolkit for automated compilation of DFT-based descriptors, J. Comput. Chem. 37 (16) (2016) 1505–1510.
[50] T. Lu, F. Chen, Multiwfn: a multifunctional wavefunction analyzer, J. Comp. Chem. 33 (5) (2012) 580–592.
[51] T. Lu, A comprehensive electron wavefunction analysis toolbox for chemists, multiwfn, J. Chem. Phys. 161 (8) (2024).
[52] E.J. Baerends, N.F. Aguirre, N.D. Austin, J. Autschbach, F.M. Bickelhaupt, R. Bulo, C. Cappelli, A.C.T. van Duin, F. Egidi, C. Fonseca Guerra, A. Förster, M. Franchini, T.P.M. Goumans, T. Heine, M. Hellström, C.R. Jacob, L. Jensen, M. Krykunov, E. van Lenthe, A. Michalak, M.M. Mitoraj, J. Neugebauer, V.P. Nicu, P. Philipsen, H. Ramanantoanina, R. Rüger, G. Schreckenbach, M. Stener, M. Swart, J.M. Thijssen, T. Trnka, L. Visscher, A. Yakovlev, S. van Gisbergen, The Amsterdam modeling suite, J. Chem. Phys. 162 (16) (2025) 162501.
[53] F. Heidar-Zadeh, M. Richer, S. Fias, R.A. Miranda-Quintana, M. Chan, M. Franco-Pérez, C.E. González-Espinoza, T.D. Kim, C. Lanssens, A.H.G. Patel, X.D. Yang, E. Vöhringer-Martinez, C. Cárdenas, T. Verstraelen, P.W. Ayers, An explicit approach to conceptual density functional theory descriptors of arbitrary order, Chem. Phys. Lett. 660 (2016) 307–312.
[54] K. Momma, F. Izumi, VESTA 3 For three-dimensional visualization of crystal, volumetric and morphology data, J. Appl. Cryst. 44 (6) (2011) 1272–1276.
[55] A. Kokalj, XCrySDen-a new program for displaying crystalline structures and electron densities, J. Mol. Graph. Modell. 17 (3–4) (1999) 176–179.
[56] A. Kokalj, Computer graphics and graphical user interfaces as tools in simulations of matter at the atomic scale, Comp. Mater. Sci. 28 (2) (2003) 155–168.
[57] W. Humphrey, A. Dalke, K. Schulten, VMD – Visual molecular dynamics, J. Mol. Graph. 14 (1996) 33–38. .
[58] G. Henkelman, A. Arnaldsson, H. Jónsson, A fast and robust algorithm for Bader decomposition of charge density, Comput. Mater. Sci. 36 (3) (2006) 354–360.

[59] E. Sanville, S.D. Kenny, R. Smith, G. Henkelman, Improved grid-based algorithm for Bader charge allocation, J. Comp. Chem. 28 (5) (2007) 899–908.
[60] W. Tang, E. Sanville, G. Henkelman, A grid-based Bader analysis algorithm without lattice bias, J. Phys.: Condens. Matter 21 (8) (2009) 084204.
[61] M. Yu, D.R. Trinkle, Accurate and efficient algorithm for Bader charge integration, J. Chem. Phys. 134 (6) (2011).
[62] A. Otero-de-la Roza, M.A. Blanco, A.M. Pendás, V. Luaña, Critic: a new program for the topological analysis of solid-state electron densities, Comput. Phys. Commun. 180 (1) (2009) 157–166.
[63] A. Otero-de-la Roza, E.R. Johnson, V. Luaña, Critic2: a program for real-space analysis of quantum chemical interactions in solids, Comput. Phys. Commun. 185 (3) (2014) 1007–1018.
[64] D. Kozlowski, J. Pilme, New insights in quantum chemical topology studies using numerical grid-based analyses, J. Comput. Chem. 32 (15) (2011) 3207–3217.
[65] G. Kresse, J. Hafner, Ab initio molecular dynamics for liquid metals, Phys. Rev. B 47 (1) (1993) 558.
[66] G. Kresse, J. Furthmüller, Efficiency of ab-initio total energy calculations for metals and semiconductors using a plane-wave basis set, Comput. Mater. Sci. 6 (1) (1996) 15–50.
[67] G. Kresse, J. Furthmüller, Efficient iterative schemes for ab initio total-energy calculations using a plane-wave basis set, Phys. Rev. B 54 (16) (1996) 11169.
[68] G. Kresse, J. Hafner, Ab initio molecular-dynamics simulation of the liquid-metal–amorphous-semiconductor transition in germanium, Phys. Rev. B 49 (1994) 14251–14269.
[69] W. Yang, R.G. Parr, R. Pucci, Electron density, Kohn–Sham frontier orbitals, and Fukui functions, J. Chem. Phys. 81 (6) (1984) 2862–2863.
[70] T. Fievez, N. Sablon, F. De Proft, P.W. Ayers, P. Geerlings, Calculation of Fukui functions without differentiating to the number of electrons. 3. local Fukui function and dual descriptor, J. Chem. Theory Comput. 4 (7) (2008) 1065–1072.
[71] P. Fuentealba, C. Cardenas, R. Pino-Rios, W. Tiznado, Topological Analysis of the Fukui Function, Springer International Publishing, Cham, 2016, pp. 227–241.
[72] J.P. Perdew, R.G. Parr, M. Levy, J.L. Balduz, Jr., Density-functional theory for fractional particle number: derivative discontinuities of the energy, Phys. Rev. Lett. 49 (23) (1982) 1691–1694.
[73] M. Berkowitz, Density functional-approach to frontier controlled reactions, J. Am. Chem. Soc. 109 (1987) 4823–4825.
[74] P.W. Ayers, R.G. Parr, Variational principles for describing chemical reactions: the Fukui function and chemical hardness revisited, J. Am. Chem. Soc. 122 (9) (2000) 2010–2018.
[75] C. Cárdenas, W. Tiznado, P.W. Ayers, P. Fuentealba, The Fukui potential and the capacity of charge and the global hardness of atoms, J. Phys. Chem. A 115 (11) (2011) 2325–2331.
[76] C. Cardenas, The Fukui potential is a measure of the chemical hardness, Chem. Phys. Lett. 513 (1–3) (2011) 127–129.
[77] T. Gómez, P. Fuentealba, A. Robles-Navarro, C. Cárdenas, Links among the Fukui potential, the alchemical hardness and the local hardness of an atom in a molecule, J. Comput. Chem. 42 (23) (2021) 1681–1688.
[78] E. Osorio, M.B. Ferraro, O.B. Oña, C. Cardenas, P. Fuentealba, W. Tiznado, Assembling small silicon clusters using criteria of maximum matching of the Fukui functions, J. Chem. Theory Comput. 7 (12) (2011) 3995–4001.
[79] M. Munoz, C. Cardenas, How predictive could alchemical derivatives be?, PCCP 19 (24) (2017) 16003–16012.
[80] M. Muñoz, A. Robles-Navarro, P. Fuentealba, C. Cárdenas, Predicting deprotonation sites using alchemical derivatives, J. Phys. Chem. A 124 (19) (2020) 3754–3760.
[81] N.D.M. Hine, J. Dziedzic, P.D. Haynes, C.-K. Skylaris, Electrostatic interactions in finite systems treated with periodic boundary conditions: application to linear-scaling density functional theory, J. Chem. Phys. 135 (20) (2011).
[82] C.A. Rozzi, D. Varsano, A. Marini, E.K.U. Gross, A. Rubio, Exact Coulomb cutoff technique for supercell calculations, Phys. Rev. B 73 (20) (2006) 205119.
[83] M.J. Rutter, Charged surfaces and slabs in periodic boundary conditions, Electron. Struct. 3 (1) (2021).
[84] M.R. Jarvis, I.D. White, R.W. Godby, M.C. Payne, Supercell technique for total-energy calculations of finite charged and polar systems, Phys. Rev. B 56 (23) (1997) 14972.
[85] All information about the patch is available at https://github.com/aradi/SCPC-Method,
[86] V. Wang, N. Xu, J.-C. Liu, G. Tang, W.-T. Geng, VASPKIT: A user-friendly interface facilitating high-throughput computing and analysis using VASP code, Comput. Phys. Commun. 267 (2021) 108033.
[87] Scripts are available at https://theory.cm.utexas.edu/vtsttools/scripts.html,
[88] P.E. Blöchl, Projector augmented-wave method, Phys. Rev. B 50 (24) (1994) 17953.
[89] G. Kresse, D. Joubert, From ultrasoft pseudopotentials to the projector augmented-wave method, Phys. Rev. B 59 (3) (1999) 1758.
[90] J.P. Perdew, K. Burke, M. Ernzerhof, Generalized gradient approximation made simple, Phys. Rev. Lett. 77 (18) (1996) 3865.
[91] H.J. Monkhorst, J.D. Pack, Special points for Brillouin-zone integrations, Phys. Rev. B 13 (12) (1976) 5188.
[92] S.L. Dudarev, G.A. Botton, S.Y. Savrasov, C.J. Humphreys, A.P. Sutton, Electron-energy-loss spectra and the structural stability of nickel oxide: an LSDA+ U study, Phys. Rev. B 57 (3) (1998) 1505.
[93] K.V. Sopiha, O.I. Malyi, C. Persson, P. Wu, Chemistry of oxygen ionosorption on SnO2 surfaces, ACS Appl. Mater. Interface. 13 (28) (2021) 33664–33676.